ECCOMAS Congress 2016
VII European Congress on Computational Methods in Applied Sciences and Engineering
M. Papadrakakis, V. Papadopoulos, G. Stefanou, V. Plevris (eds.)
Crete Island, Greece, 5–10 June 2016

SIMULATIONS OF BLAST WAVE PROPAGATION IN OPEN AND CLOSED SPACE

Natalya N. Fedorova[1,2], **Svetlana A. Valger**[1], **Yulia V. Zakharova**[1,2]

[1]Novosibirsk State University of Architecture and Civil Engineering (Sibstrin),
113, Leningradskaya st., Novosibirsk, Russia,
e-mail: swetla-ya@mail.ru

[2] Khristianovich Institute of Theoretical and Applied Mechanics SD RAS
4/1 Institutskaya, Novosibirsk, Russia
{nfed,julsemen}@itam.nsc.ru

Keywords: blast, explosion, shock waves, numerical modelling, cityscape

Abstract. *The paper presents results of 3D numerical simulations of shock wave spreading in cityscape area modeled by prismatic bodies placed on a flat plate and inside a closed room. ANSYS Autodyne software is used for the computations. Four different test cases are investigated numerically. The simulation results have been compared to experimental data. The ability of two numerical schemes is studied to correctly predict the pressure history in several gauges placed on walls of obstacles.*
.

1 INTRODUCTION

Nowadays, a lot of industrial accidents accompanied by explosions are happening throughout the world. Also, increase in the number of terrorist acts committed by means of explosions is observed. For improving safety of buildings and structures it is necessary to raise their resistance to explosive effects, as well as to be able to predict degree of potential damage upon explosive loads of various intensities [1 - 3]. One of the principal goals in designing the structure resistant to explosive effects is to determine the dynamic response of structures to the impact of the blast wave. To this end, the transient pressure loads on the walls of the civil engineering structures are to be determined.

The simulation of explosion is highly complicated, involving an explosion causing the shock wave propagation in air and then interaction with a structure. In recent years, many efforts have been devoted to the development of reliable methods and algorithms for a more realistic analysis of structures subjected to blast loading. Blast predictions are most commonly conducted in one of two ways: simplified analytical and engineering methods [4 - 6] or sophisticated CFD models [7 -8].

The engineering-level techniques permit one to estimate an explosive shock impact only for isolated buildings. The complexity of the building, the presence of nearby structures and the surrounding environment can't be taken into account. To overcome these limitations, various CFD instrumentations are used for blast impact on the civil engineering objects including in-house and commercial software. Advanced computer aid engineering (CAE) software techniques combined with the latest methods of discrete three-dimensional city modeling permits one to simulate and analyze the effects of explosions in urban areas with a precision which previously was not possible [9, 10].

In the previous papers by the authors [11, 12], the adaptation of LS-DYNA and AUTODYN software was performed for the 3D problem of the blast wave impact on the single prism installed on the flat plate. Comparison of the simulation results to the experimental data [13] has shown that LS-DYNA and AUTODYN allow one to perform numerical modelling of explosive impact on the environment with an acceptable accuracy. The simplified engineering formulas gave a good coincidence with the experimental data only for the gauges situated on the windward surface of the model.

In the paper, ANSYS AUTODYN software was tested on the problems of blast wave propagation in the open and closed spaces. The simulation results are compared to the experimental and numerical data [13 - 17]. The ability of two numerical schemes [18-20] is studied to predict the pressure history in gauges placed on walls of obstacles.

2 PROBLEM SETUP

Four different test cases are investigated numerically: three of them are for an open space with prismatic bodies placed on a flat plate, and the fourth is for the closed space with/without opening. In all the computations performed, the computational domains were the volume of air with the initial parameters corresponding to normal atmospheric conditions, namely, density ρ = 1.225 kg/m^3, temperature T = 298.15 K, static pressure P = 101325 Pa, the heat capacity C_p = 1004 J/kg·K. The geometries, problem setup and computational grids for the test cases are described below.

2.1 Test Case #1

The example has been taken from [13]. The prismatic body with 0.163x0.061 m cross-section and of 0.163 m height is placed on the flat plate. The charge of 23.7 g Demex explosive that corresponds to 27.26 g TNT is situated above the ground on height of 0.1 m and 1.5

m distance from the body. The geometry is shown in Figure 1. Two pressure gauges T1 and T2 are installed on the windward and leeward faces of the prism. Because of problem symmetry, only half of the physical domain was modeled to reduce the computation costs.

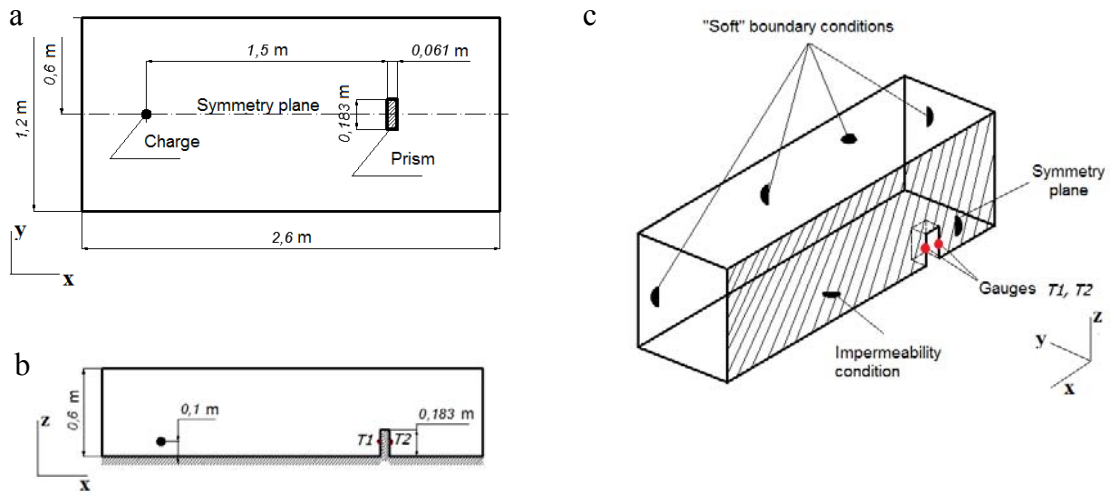

Figure 1: Plane view (a), central *y* cross-section (b) and 3D computational domain (c) for the test case #2

2.2 Test Case #2

This case has no any experimental data. The example was proposed and studied numerically in [14]. The geometry of Case #2 is shown in Figure 2. Two prisms of different heights are installed on the plate substrate. At initial moment, the charge of 189 g TNT explosive is detonated at the point placed on the ground by 0.2 m distance from the front face of the smaller prism. The virtual gauges are put on the windward and leeward faces of the prisms. This case has also been computed for a half of the domain taking into account symmetry of the problem.

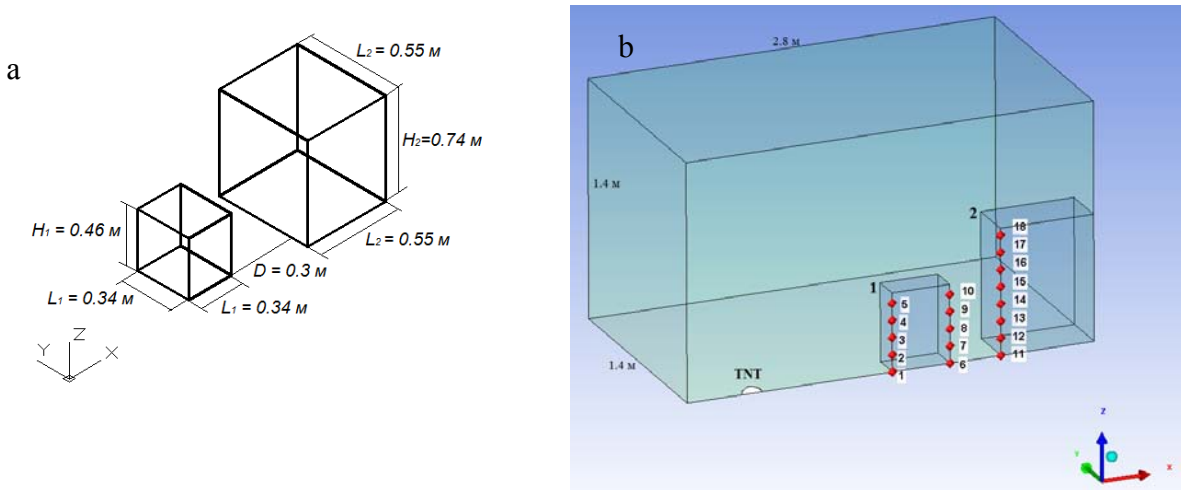

Figure 2: Prism geometry (a), and computational domain for the test Case #2

2.3 Test Case #3

The test Case #3 experimentally studied in [15, 16]. Seven building shown in Figure 3 as A - F placed on the plate ground surface were imitating a cityscape. The heights prisms were as follows: $H_A = H_G = 0.45$ m; $H_B = H_C = H_E = 0.4$ m; $H_D = H_F = 0.3$ m. The TNT charge of 16.0 g capacity is detonated at the point located by 0.04 m above the ground between buildings C and F. The distance between adjacent objects is less than or comparable to a linear scale of the prisms. In contrast to the test problems #1 and #2, for this configuration simulation cannot be carried out in a symmetrical approach and requires full 3D consideration. The static pressure behavior was recorded in several gauges placed at the prism walls and compared to the experimental data [15].

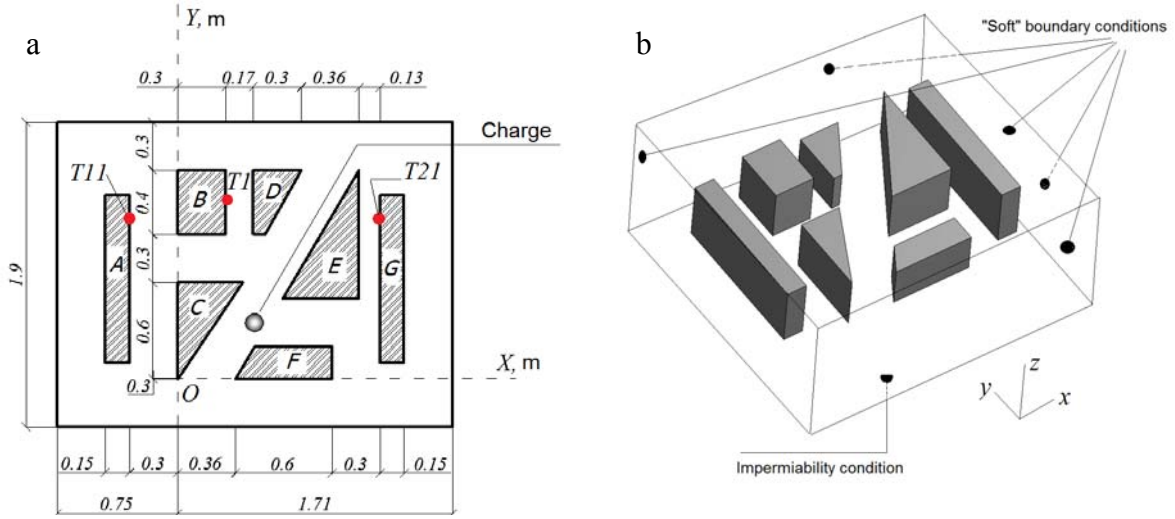

Fig. 3. Plane (a) and isometric (b) views of test Case #3 geometry

2.4 Test Case #4

In the test Case #4, (Figure 4), the internal explosions of TNT charge are studied for the closed cubical region of $3 \times 3 \times 3$ m without and with ventilation opening. The numerical simulation was carried out under the conditions of the experiments performed at the National Building Research Institute, Technion, Haifa, Israel [17]. The contact pressure was recorded during the computations at gauges shown in the Figure 4.

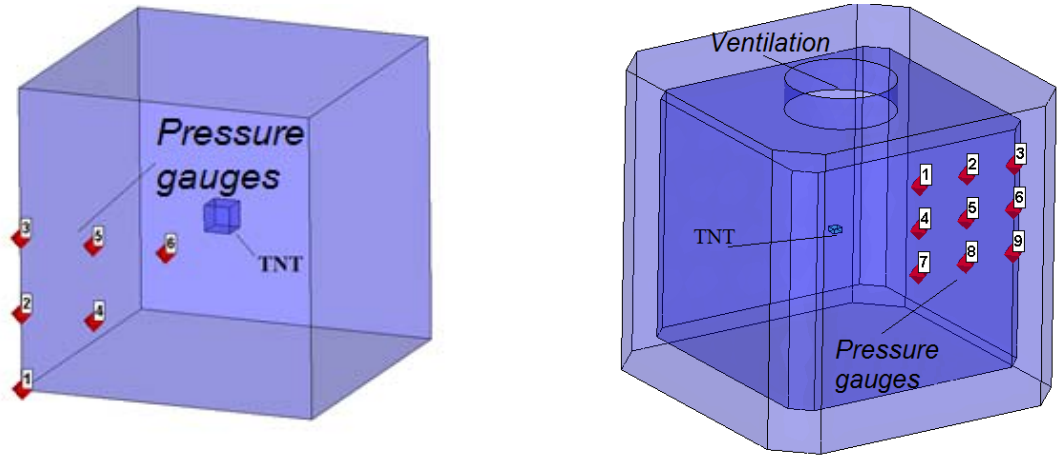

Figure 4: Geometries for test Case #4 without (a) and with ventilation (b)

3 MATHEMATICAL MODEL AND METHODS OF COMPUTATIONS

The air region was generated around the prismatic bodies in Cases #1 - 3 including the explosive charge. For the Case #4, the computational domain was confined by the room walls. At the initial time $t = 0$ the charge detonates, and detonation and shock wave spreads in open or closed space. Blast wave formation and propagation was computed with AUTODYN ANSYS 15.0 software on the basis of a hydrodynamic multi-material approach. The air and TNT properties used in the computations were retrieved from the standard AUTODYN library. The 3D Euler equations were used for computations complemented with the ideal gas equation of state for air and the JWL equation of state [21] for TNT:

$$\rho = A\left(1-\frac{\lambda\eta}{R_1}\right)e^{-\frac{R_1}{\eta}} + B\left(1-\frac{\lambda\eta}{R_2}\right)e^{-\frac{R_2}{\eta}} + \lambda\rho e, \qquad (1)$$

The values of the empirical constants A, B, R1, R2, □ are shown in Table1, e is the specific internal energy and □ = □/□0 is the relative specific density.

Constant	*A,* kPa	*B,* kPa	R_1	R_2	λ	*E*, kJ/m^3	kg/m^3
Value	$3{,}7377\cdot10^8$	$3{,}7471\cdot10^6$	4,15	0,9	0,35	$6{,}0\cdot10^6$	1630

Table 1: Values of empirical constants in (1).

At the external boundaries chosen far enough from region of interest, so called “soft” boundary conditions were set. All walls were supposed to be non-deformable, and “symmetry” conditions were used at the walls that guaranteed the absence of the flow through these boundaries. The second-order Godunov [18, 19] and FCT [20] finite-difference schemes were applied for space approximation. For the temporal approximation, the explicit scheme of the second order was used in compliance with the stability conditions. As the initial process of detonation in the open space is well described in the assumption of axial symmetry, to the moment when the primary shock wave reaches the plate or some prism surface, it is carried out in a 2D approximation. Then, the data obtained in the 2D calculations are interpolated at a 3D computational domain and simulations were continuing taking into account the shock wave interaction with the substrate and prism surfaces.

4 RESULTS OF COMPUTATIONS

4.1 Test Case #1

The grid convergence study was first performed using the second order sequel to Godunov’s type finite difference scheme. Four various grids with hexagonal cells of equal size were used. Table 2 shows the details of the grids.

Grid #	Cell size in *x*-direction, cm	Cell size in *y*-direction, cm	Cell size in *z*-direction, cm	*Nx*	*Ny*	*Nz*	Total cell number
1	1	1	1	260	60	60	9.36E+05
2	0.5	1	1	520	60	60	1.872E+06
3	0.25	1	1	1040	60	60	3.744E+06
4	0.5	0.5	0.5	520	120	120	7.488E+06

Table 2: Computational grids for test case #1.

The computed pressure history in the T1 gouge placed on the windward prism face presented in Figure 5 shows that all grids give similar results. All further computations were performed on the grid #4.

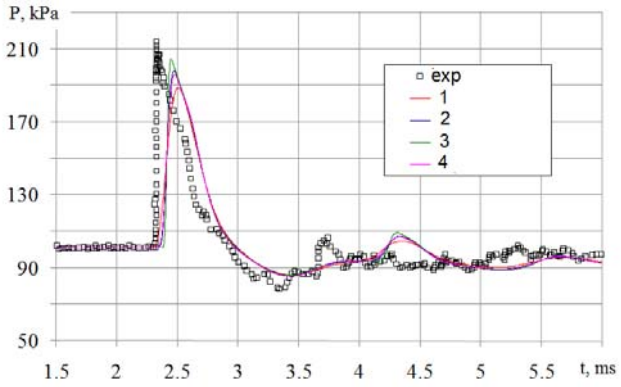

Figure 5: Grid convergence study for test case #1

Figure 6 shows the computed static pressure field in a symmetry plane in various time moments. Pressure histories written in gauges T1 and T2 are shown in Figure 7. As can be seen from Figure 6, a that corresponding t = 0.018 ms, shock (1) is reflected regularly from the surface. In Figure 6, b one can see the irregular mode of shock reflection from the substrate. The wave front consisted of the original shock (1) and the Mach stem (2) propagates toward the prism. At the same time, reflected shocks (3) and (4) are moving toward the epicenter. After their interaction, a new secondary shock (5) is formed. In Figure 6, f pressure contours are shown at the moment when the primary shock front reaches the front wall of the prism. After reflection, the shock (6) appears, and negative phase starts with pressure level lower that 1 atm. Figures 6, g, h show the diffraction of shock wave (2) along the prism walls and spreading of reflected shock (6) toward the epicenter. Further, shocks (6) and (5) interact that lead to formation of secondary wave of lower intensity.

In Figure 7, besides the experimental data, three computation data are presented. The two of lines are obtained on the basis of 3D Euler equation computations using Godunov-type scheme of the second approximation order [18, 19] and FCT scheme [20]. The data obtained with empirical CONWEP function [4]. It can be seen that engineering-based approach permits one to predict the pressure maximum and shock arrival time to the frontal face of the prism which is in direct view of the explosion epicenter. But the CONWEP function is not able to describe the shielding effect as well as the secondary front formation. So an implementation of this approach is only possible to determine impact of the explosion on a single building.

As Figure 7 shows, there are several pressure peaks at frontal and rare faces of the prism. The first maximum $P_{max} \approx 213$ kPa in Figure 7, a, is due to the impact of the shock (2) on the frontal face of the prism. The secondary shocks (5) and (6) cause the local maxima of 115 kPa on the plot of pressure history taken in T1 gauge. It should be noted that Godunov-type scheme underpredicts the pressure peaks and gives some delay in shock arrival moments on the windward and leeward faces. The first pressure peak on the leeward face is caused by action of primary shock wrapped the prism surface, while the second peak is due to the action of the same wave reflected from the ground surface. The second maximum is underpredicted by both schemes. Nevertheless, the plot shows that FCT scheme works better comparing the Godunov-type scheme and gives adequate prediction of the main pressure peaks and shock arrival times.

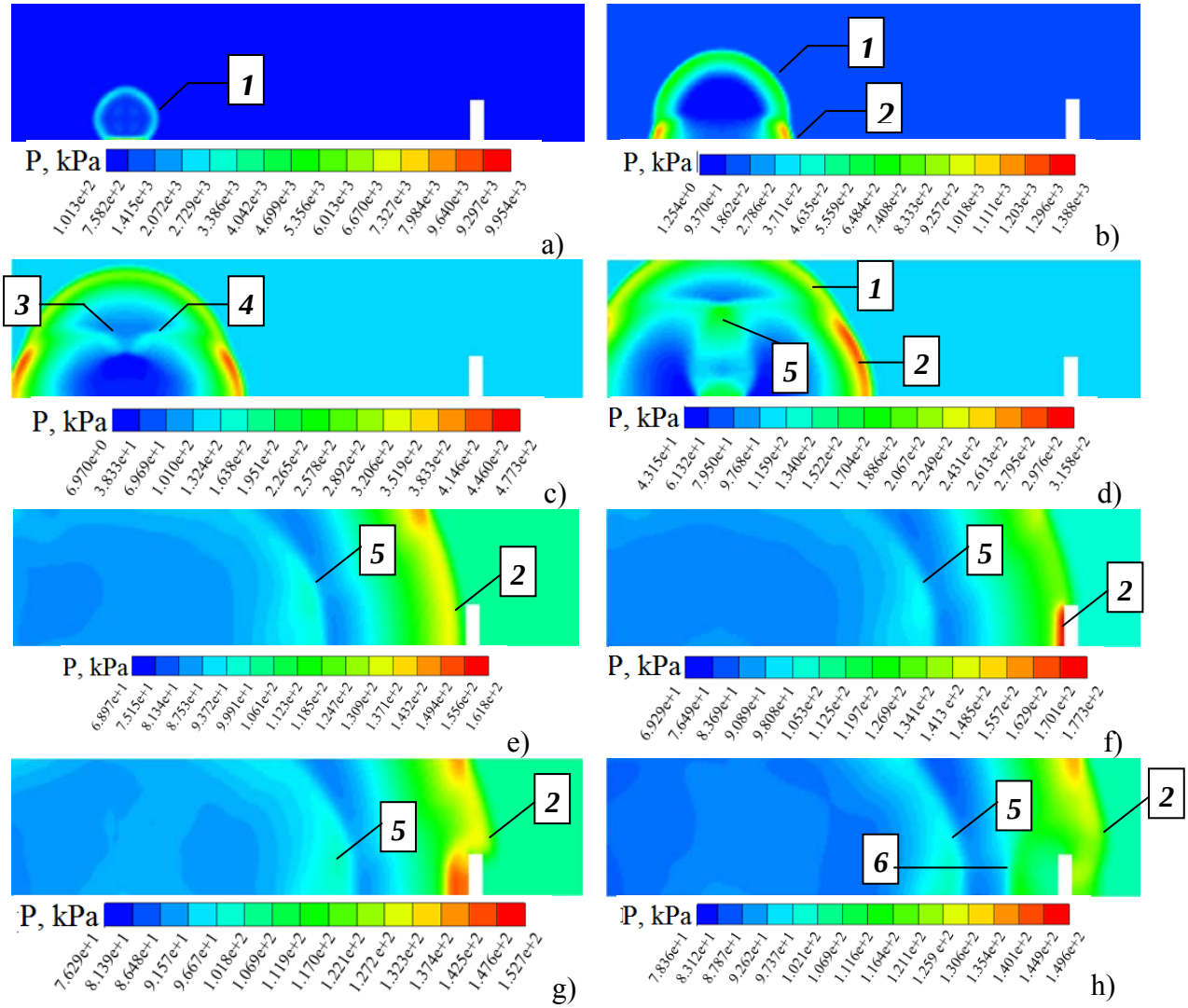

Figure 6: Instantaneous pressure fields at various time moments: 0.018 (a), 0.13 (b); 0.36 (c); 0.62 (d); 2.32 (e); 2.45 (f); 2.72 (g); 2.95 (h) ms.

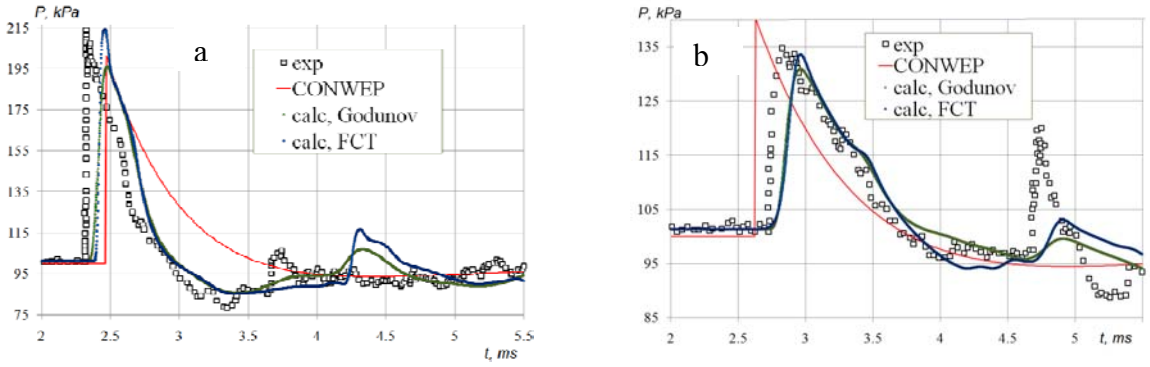

Figure 7: Computed (lines) and experimental (symbols) pressure history in T1 (a) and T2 (b) gauges

4.2 Test Case #2

The computation domain was of 1.4 × 2.8 × 1.4 m size and consisted of 3.8 million cells with the cell size of 5 mm. Visualization of pressure contours available during the post-processing stage allows a better understanding of the complex process of blast pressure interaction with a group of buildings. Figure 8 shows the computed static pressure at the ground level ($z = 0$) for different time moments after detonation. The pressure histories in the gauges placed on the front walls of the buildings are shown in Figure 9.

From the figures, it could be seen that the shock (1) is spherically propagating till it reaches the front surface of the first building at time t=0.076 ms. Pressure history written in gauges on front face of the first building shows that maximal pressure of 8.5e+3 kPa is observed in gauge #1. The shock (1) interacts with shock (2) formed as a result of reflection. The common wave front propagates along the wall and wraps the whole building 1. During the diffraction, in a vicinity of the front face of the first building pressure falls below the atmospheric level. High pressure levels shown in figures by red circles are observed in triple points of shock interactions and reflections from the walls and symmetry line. This pressure rise causes the second peaks observed in gauges 1-5 at t ≈ 0.8 ms. After shock coming to the frontal face of the second building, all the gauges placed on the surface show significant pressure increase.

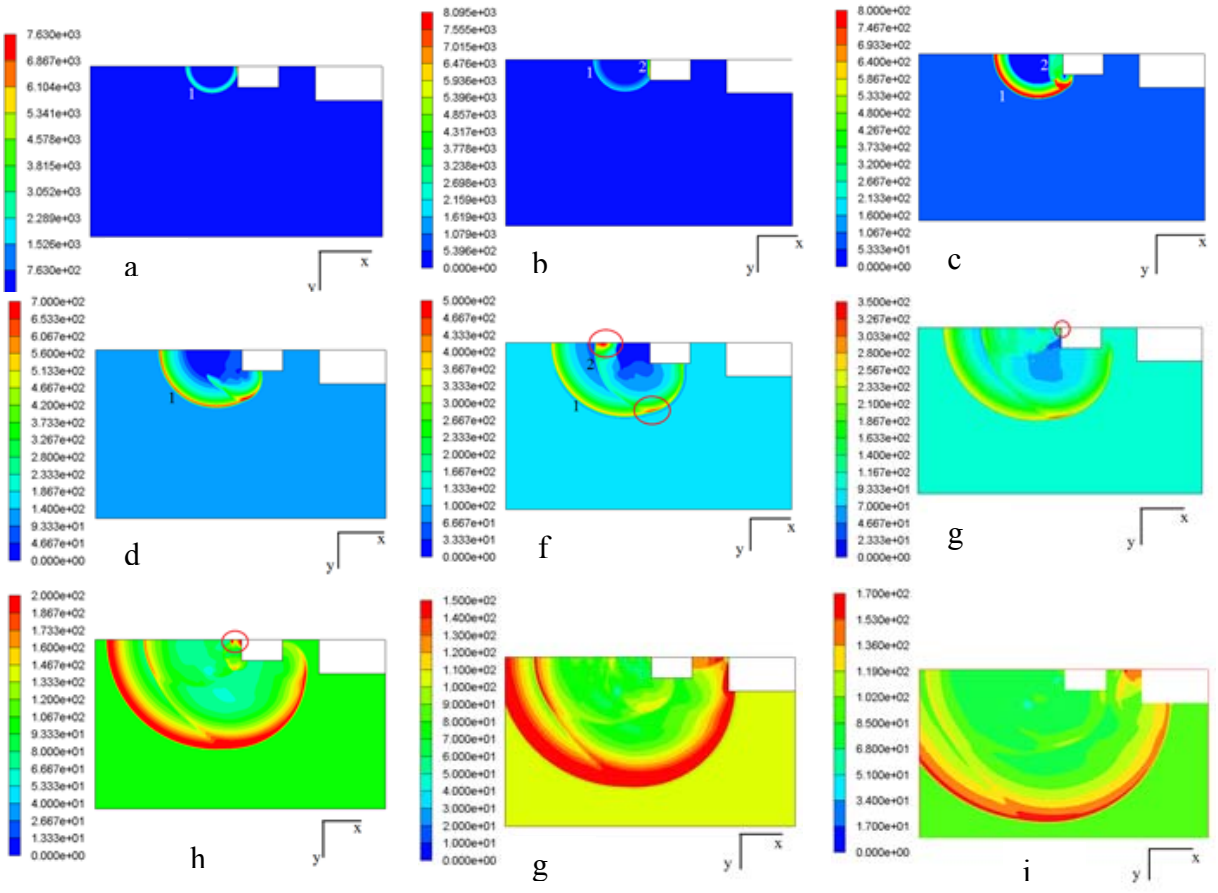

Figure 8: Instantaneous pressure fields for test case 2 at various time moments: 0.07 ms (a), 0.1 ms (b); 0.2 ms (c); 0.3 ms (d); 0.5 ms (e); 0.8 ms (f); 1.04 ms (g); 1.4 ms (h), 1.8 ms (i).

Nevertheless, it should be noted that amplitudes of the peaks here is lower by the order of magnitude comparing those on the frontal face of the first building due to the shield effect. Because of a narrow space between the first and the second buildings, some additional shocks of lower intensity arise due to multiple reflections from the canyon walls. The traces of these secondary shocks can be seen in the pressure history plots shown in Figure 9, b.

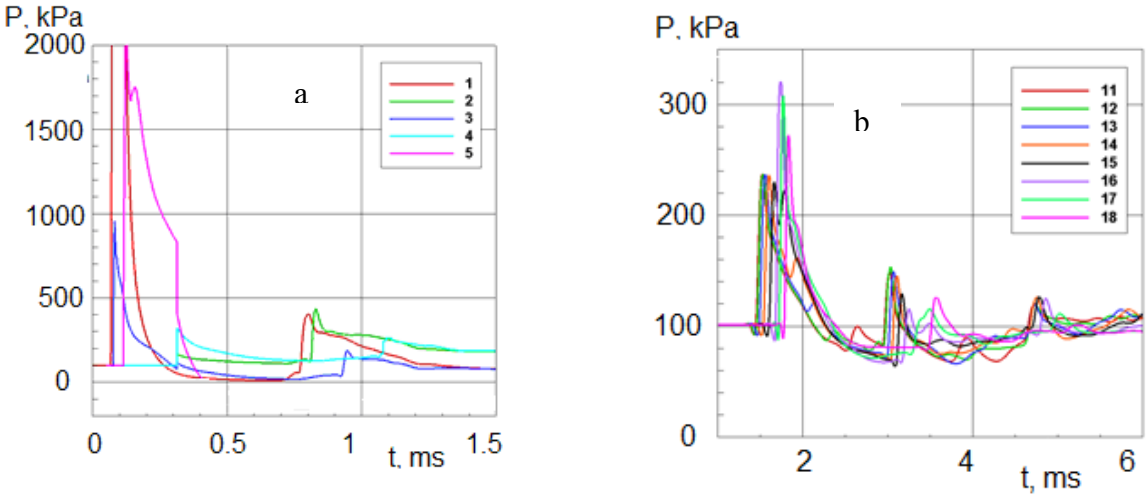

Figure 9: Computed (lines) pressure history in gauges places on the front face of Building 1 (a) and front face of Building 2 (b).

4.3 Test Case #3

The computations of this test case were performed in the computational domain with about 6 million hexa-cells each of 1×1×1 cm size.

Let's consider the shock-wave structure in the vicinity of the building complex. In Figure 10 the instantaneous static pressure contours in a horizontal plane-section z = 0.105 m. Spherical shock (1), formed as a result of detonation propagating in an open space till it reaches the corner of the building F (Figure 10, a). After reflection, the shock wave intensity is about 6 MPa. In some time moment the shock (1) falls on the wall of the building C and corner of the building E and reflects by irregular manner forming the triple points denoted by 3, 4 and 5 in Figure 10, b . The shock (2) arises after reflection of the shock (1) from the building C and propagates toward the epicenter. The interaction of shocks (6) and (2) results in formation of the shock (7). At the same time, as Figures 10, c, d show, the shock (2) goes around a sharp corner of the building C and interacts with the shock (1).

In Figures 10, e- one can see how the joint front of shocks 1 and 2 comes through the channel between building B and D. The action of this front leads to a fast pressure rise in the gauge T1 that can be observed in Figure 11,a. The second pressure peak is formed due to action of secondary shocks (11) formed in the epicenter in result of numerous interactions of reflected shocks.

The first peak is pressure history plot in T21 gauge (Figure 11,b) is a result of shock (8) passing between buildings E and G. Afterwards, a negative phase is observed. Corresponding rarefaction wave formed in result of shock diffractions can be seen in Figure 10,h.

Further wave structure analysis is complicated by a large number of shocks and rarefaction waves formed in result of numerous interferences, reflections and diffraction of the waves.

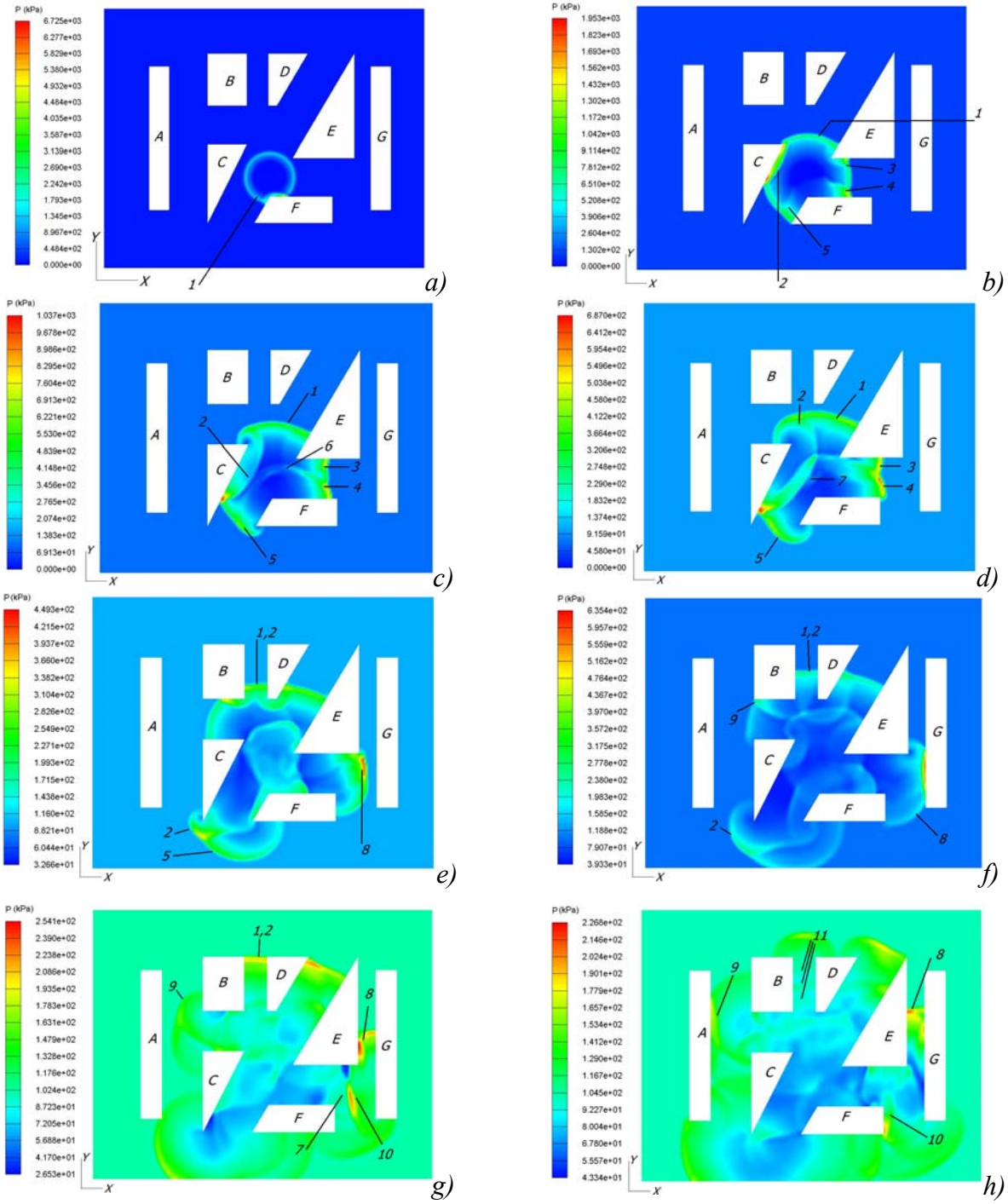

Figure 10: Instantaneous pressure fields for test case #3 at various time moments: 0.1 (a), 0.2 (b); 0.3 (c); 0.4 (d); 0.7 (e); 0.9 (f); 1.3 (g); 1.7 (h) ms.

The comparison of computed results and experimental data is shown in Figure 11. The symbols stand for experimental data [15] and the lines show the pressure history computed with two different schemes. The picture shows that both schemes predict the pressure loads on the building walls including positive and negative phases. The FCT scheme, as in previous case, is better in predicting the peak amplitudes and secondary waves.

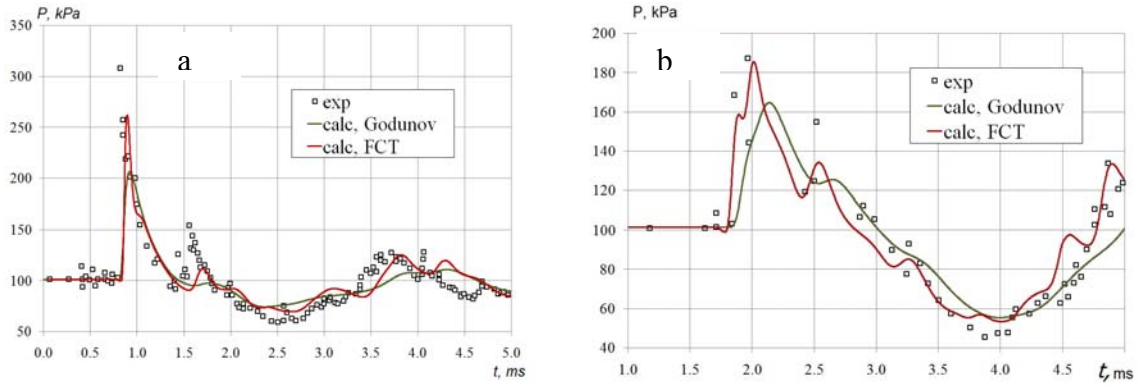

Figure 11: Computed (lines) and experimental (symbols) pressure history in T1 (a) and T21 (b) gauges.

4.4 Test Case #4

First, 3D modeling of the explosion was carried out of for the 16 kg TNT charge located in the center of the room of 300×300×300 cm size in fully confined space. During the calculation, the static pressure history was recorded at control points located on one of the walls which were assumed to be non-deformable. Computational grid for the task contained 343,000 cells. The characteristic size of the computational cell was 4 cm.

Figure 12 presents the pressure contours on the wall (x=0) showing the shock wave propagation and reflection. Figure 13, a presents computed pressure histories at various gauges on the wall $x = 0$. It can be seen that because of a big charge mass, very high pressure levels were obtained in this case.

The blast wave expands from the epicenter and first comes to the gauge #6 situated in the wall center. As the shock spreads along the wall, the pressure rises in gauges #4 and 5 while decreases in gauge #6. In time moment $t = 1.5$ ms shock front reaches wall edges and reflects from perpendicular walls that lead to significant increase of the pressure peak. The highest pressure level of about 20 MPa is observed at gauge #1 situated at a very corner of the room. After reflection from the wall, the shock front moves toward the room center, and after symmetrical reflection, the whole process is repeated, but the second pressure spikes are lower and average pressure in the room increases.

As the next stage, computations were performed under the conditions of [17] for the TNT charge, located inside the room of 290×290×270 cm with the vent opening of 120 cm diameter in the ceiling. All the internal corners of the room had a 20 cm chamfer. In the center of the room TNT explosive was located. The mass of the explosive chards was varying (Table 4). It the experiment, the static pressure was measured in nine sensors installed on one of room walls. Computational grid for the task contained 2 million cells with the size of 2 cm.

Charge mass, kg	Charge dimensions, mm		
	$\mathbf{L_1}$	$\mathbf{L_2}$	$\mathbf{L_3}$
0.5	104	67	52
1	134	104	52
1.5	156	134	52

Table 4: Charge parameter for Test case #4.

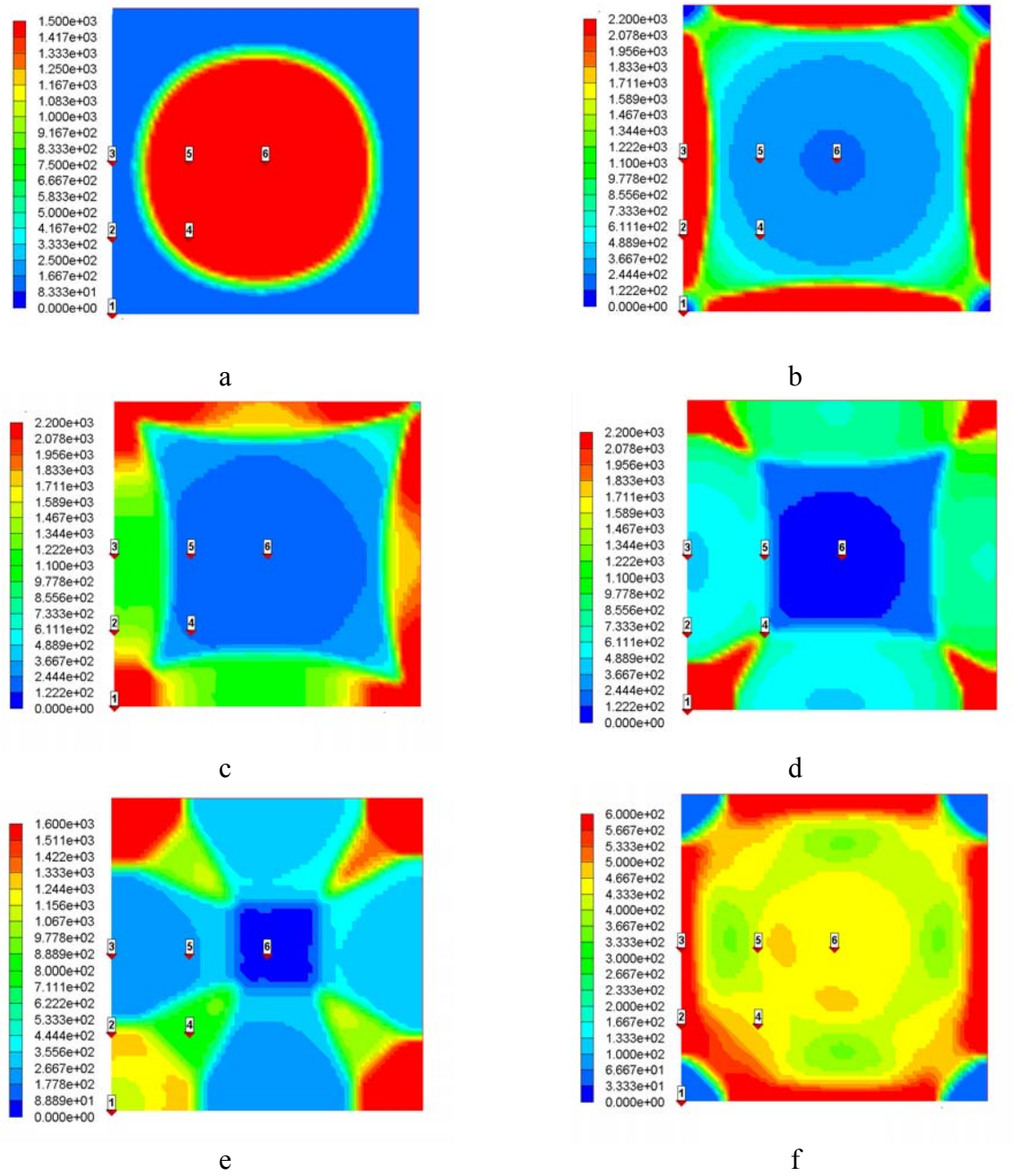

Figure 12: Instantaneous pressure fields for test case #4 (without ventilation) at various time moments: 0.9 (a), 1.5 (b); 1.7 (c); 1.97 (d); 2.3 (e); 4.8 (f) ms.

The computed pressure history for the charge mass of 0.5 kg is shown in Figure 13, b, and pressure plots at various time moments are presented in Figure 14. Because of significantly smaller charge mass, the amplitude of pressure spikes is much lower than in the previous computations. The highest pressure is observed in the gauge #7 located close to the wall center. Static pressure contours at the wall $z = 0$ for test Case #4 with vent, m_{TNT} =0.5 kg at various time moments are presented in Figure 14. At the beginning, the whole shock wave structure is similar to that observer for a confined room. But due to the presence of vent opening, big part of the shock wave energy goes out of the room, an after the second reflection, pressure equalized, but the third pressure spike is observed in the gauge #7. The computed data were compared to experimental data [17] and a satisfactory agreement was obtained.

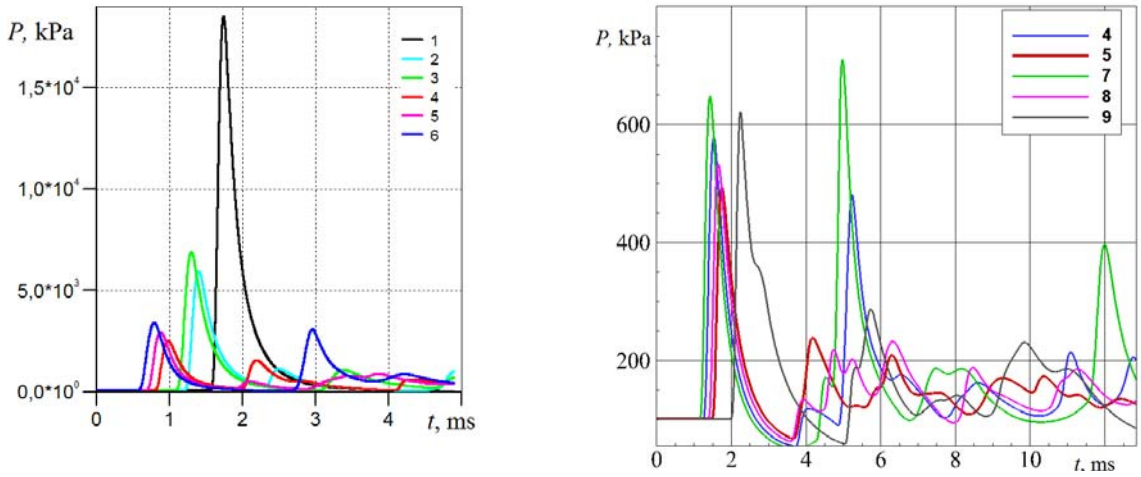

Figure 13: Computed pressure history at various gauges for test Case #4, m_{TNT}=16 kg without vent (a) and m_{TNT} =0.5 kg with vent (b).

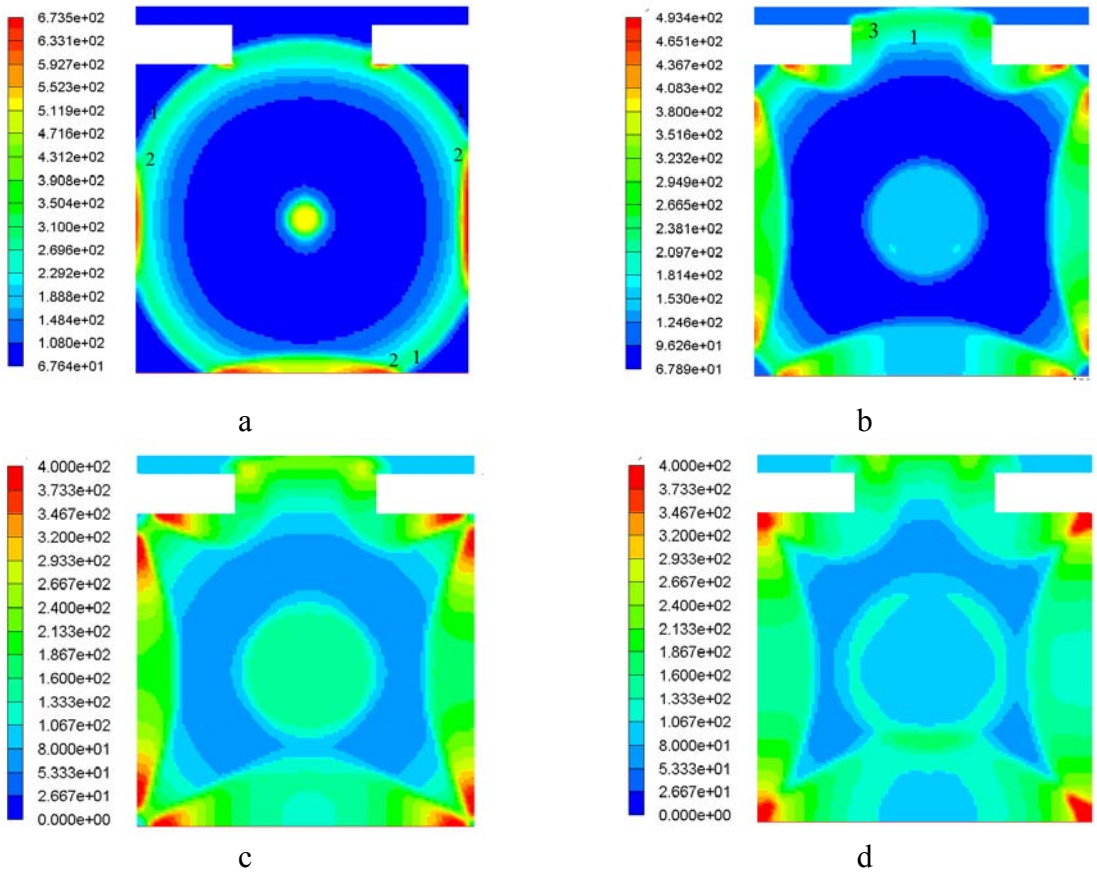

Figure 14: Instantaneous pressure fields for test case #4 (with ventilation) at various time moments: 1.4 (a), 1.9 (b); 2.0 (c); 2.2 (d) ms.

5 CONCLUSIONS

- Four different test cases of explosive charge detonation and blast wave propagation in open and fully or partly confided space were investigated numerically using ANSYS Autodyn software;

- The list of test cases includes: (1) single prismatic body installed on the flat substrate; (2) two prismatic body of different size installed on a flat plate; (3) generic cityscape of several prismatic bodies installed on a flat plate; (4) fully or partly confined room.
- On a basis of simulation results, a complex wave structure was analyzed, and all the peculiarities of flows and pressure history records on building / room walls were described and explained.
- Juxtaposition of simulation results with experimental data available were performed showing a satisfactory agreement.
- The comparison of two numerical scheme abilities has shown the better FCT properties to predict fine flow details
- The use of ANSYS AUTODYN tool can provide an effective approach to determining blast loads in an urban environment.
- The results indicate the necessity to take all the surrounding buildings into account when computing the blast loads on buildings in an urban environment.

ACKNOWLEDGMENTS

The work was supported by the Ministry of Education of the Russian Federation (Project No. 211, Task No. № 2014/140 for executing scientific activities within the basic part of government order) and by Russian Foundation for Basic Research, grant № 15-07-06581.

REFERENCES

[1] Donald O. Dusenberry, ed., *Handbook of blast resistant design of buildings.* John Wiley & Sons, 2010.

[2] W. E. Baker, P. A. Cox, P. S. Westine, J. J. Kulesz, R, A. Strehlow, *Explosion Hazards and Evaluation*. Elsevier Scientific Publishing Company, 1983.

[3] T. Ngo, P. Mendis, A. Gupta, and J. Ramsay, Blast loading and blast effects on structures - an overview. *EJSE international*, Special Issue: Loading on structures, 76 – 91, 2007.

[4] Hyde D., *Users Guide for Microcomputer Programs CONWEP and FUNPRO – Applications of TM 5-855-1*. U.S. Army Engineer Waterways Experimental Station, Vicksburg, 1988.

[5] Kingery C.N. and Bulmash G., *Airblast Parameters from TNT Spherical Air Burst and Hemispherical Surface Burst, Report ARBL-TR-02555*, U.S. Army BRL, Aberdeen Proving Ground, MD, 1984.

[6] *Design and Analysis of Hardened Structures to Conventional Weapons Effects*. Washington, DC: The Departments of the Army, Air Force, Navy and The Defense Special Weapons Agency Defense Special Weapons Agency (DSWA), 1998.

[7] Randers-Pehrson G. *Airblast Loading Model for DYNA2D and DYNA3D. ARL-TR-1310*. Army Research Laboratory, Aberdeen Proving Ground. MD, 1997.

[8] Rose T. A. A Computational Tool for Airblast Calculations, *Air3d version 9 users' guide, Engineering Systems Department* Cranfield University, 2006.

[9] Smith, P. D. and Rose, T. A., Blast wave propagation in city streets—an overview. *Prog. Struct. Engng Mater*., **8,** 16 – 28. 2006.

[10] http://www.virtualcitysystems.de/en/114-english/references/research/352-detorba-2

[11] Valger S.A., Danilov M.N., Fedorov A.V., Fedorova N.N. The comparison of results of simulation of shock wave action on structures using ANSYS AUTODYN and LS-DYNA software // *News of Higher Educational Institutions. Construction.* No. 11 (671). 77 – 92, 2014.

[12] Fedorov A.V., Fedorova N.N., Fomin P.A., Valger S.A. *Propagation of explosive shock waves in block-up spaces*. Novosibirsk: Novosibirsk State University of Architecture and Civil Engineering (Sibstrin), 2015.

[13] Rose T.A. *An approach to the evaluation of blast loads on finite and semi-infinite structures.* PhD thesis, Engineering Systems Department, Cranfield University, Royal Military College of Science, February 2001.

[14] Remennikov A. M., Rose T. A., Modelling blast loads on buildings in complex city geometries. *Journal Computers and Structures,* **83**, (27), 2197 - 2205, 2005.

[15] Matthew A. Brittle, *Blast propagation in a geometrically complex environment. MSc dissertation*, Craneld University, Defence College of Management and Technology, Defence Academy of the UK, Shrivenham, Swindon, SN6 8LA, UK, Jul 2004.

[16] Smith P.D., Rose T.A., and Brittle M.A. Analysis of a generic cityscape using an adaptive mesh CFD code. *Proceedings of the 12th International Symposium on Interaction of the Effects of Munitions with Structures,* New Orleans, USA, 13th–16th September. 2005.

[17] V.R. Feldgun, Y.S. Karinski, I. Edri, D.Tsemakh and D.Z. Yankelevsky, On Blast Pressure Analysis Due to a Partially Confined Explosion: I – Experimental Studies. *International Journal of Protective Structures*, **2**(1), 1 – 20, 2011.

[18] S. K. Godunov, A finite difference method for the numerical computation of discontinuous solutions of the equations of fluid dynamics, *Mat. Sb*., **47**, 271–290, 1959.

[19] Van Leer B., Towards the ultimate conservative difference scheme V: a second – order sequel to Godunov‘s method. *Journ. of Comput. Phys.* **32** (1), 101 – 136, 1983.

[20] Zalesak S. T., Fully Multidimensional Flux-Corrected Transport Algorithms for Fluids. *Journal of Comp. Phys.* **31**, 335–362, 1979.

[21] Baum F.A., Orlenko L.P., Stanukevich K.P., Chelyshev V.P., Shaehter B.I. *Physics of explosion.* Moscow: Nauka, 1975.